Nanoscale

Accepted Manuscript

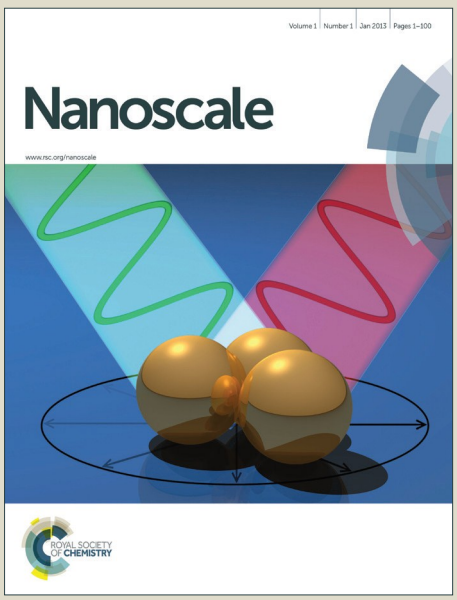

ROYAL SOCIETY OF CHEMISTRY

www.rsc.org/nanoscale

Nanoscale

RSCPublishing

ARTICLE

Cite this: DOI: 10.1039/x0xx00000x

Synergistic Effects from Graphene and Carbon Nanotubes Enable Ordered Hierarchical Structure Foams with Combination of Compressibility, Super-elasticity and Stability, and Their Potential Application as Pressure Sensors

Received 00th January 2012,
Accepted 00th January 2012

DOI: 10.1039/x0xx00000x

www.rsc.org/

Jun Kuang,[a,b] Zhaohe Dai, [a,b] Luqi Liu,[*a] Zhou Yang,[c] Ming Jin,[c] Zhong Zhang,[*a]

Nanostructured carbon materials based three-dimensional porous architectures have been increasingly developed for various applications, e.g. sensors, elastomer conductors, energy storage devices. Maintaining the architectures with good mechanical performance including elasticity, load-bearing capacity, fatigue resistance and mechanical stability is priority to realize the functions. Though graphene and CNT offer an opportunity as nanoscale building blocks, it still remains a great challenge to achieve good mechanical performance in their microarchitectures since the needing to preciously control the structure at different scale. Here, we fabricate hierarchical honeycomb-like structured hybrid foam base on both graphene and CNT. The resulting materials possess superb properties of combining high specific strength, elasticity and mechanical stability which cannot be achieved in neat CNT and graphene foams. The improved mechanical properties are attributed to the synergistic-effects-induced highly organized, multi-scaled hierarchical architectures. Moreover, together with their electrical conductivity, we demonstrated that the hybrid foams could be used as pressure sensors in artificial skin field.

Introduction

For the essential role played by cellular materials in engineering and biomechanical applications, advanced foam technologies have been heavily involved in the development of new cellular materials, by tuning their building blocks, to meet the increasing demands for high-performance materials.[1-5] In this field, nanostructured carbon materials such as carbon nanotubes (CNT) and graphene, combining extraordinary mechanical, electrical and thermal properties, hold great promise as an exceptional nanoscale building block for constructing macroscopic bulk cellular solids.[5-12] Recently, a variety of techniques such as sol-gel,[6, 13-15] hydrothermal,[9, 16] and chemical vapor deposition method,[11, 12] have been developed to fabricate various CNT and graphene based cellular solids with multi-functionality, temperature-invariant performance and ultralow density. However, though the super elasticity and strength of CNT and graphene building blocks, most of the prepared macroscopic porous architectures are generally brittle with low compression resilience ratios, as the microstructural feature also dominates the bulk mechanical response.[6, 9, 12-14, 16] Thus, efficient assembly of nanostructured carbon foams with appropriate structure is the key to fully realize the potential of building blocks in macroscopic architecture and achieve superb mechanical compressibility, elasticity and stability.

Sustained efforts for innovation have led to the development of CNT and graphene based porous macrostructures with ordered and hierarchical honeycomb-like structures as well as remarkable mechanical resilience. For instance, unlike the isotropic graphene or CNT aerogels formed by randomly stacking which were easily to collapse when subjected to compressive deformation, particularly at large strain level, [6, 9, 12-14, 16] the ultra-light free standing multi-walled nanotube aerogels with ordered honeycomb-like structure, fabricated by unidirectional freeze-casting approach, have shown excellent compression recoverable property.[8] Additionally, following the similar technique, Li D. and co-workers[10] fabricated biomimetic honeycomb-like hierarchical graphene based cellular foams by carefully controlling the carbon/oxygen atomic ratio in partially reduced graphene oxide sheets. Even though the specific elastic bending stiffness of a plate structure

is intrinsically inferior to that of tubular counterparts, the obtained graphene cellular foam still possess excellent compression resilience which attribute to the ordered structure. Given the fact that the effective properties of cellular materials are defined both by the intrinsic properties of the solid constituents and their structural geometry, thus we expect that nanostructured material foams would exhibit expected mechanical performance if the mechanical properties of solid constituents in the foams could be enhanced along with structure in this ordered, hierarchical manner.

Previous research advances have attempted to integrate the unique properties of the individual graphene sheets and carbon nanotubes into one-dimensional fibers, two-dimensional (2D) films for practical applications.[17-19] Synergistic effects were observed that hybrid materials of the graphene and CNT could exhibit greatly improved electrical, thermal conductivity and especially mechanical properties, compared with those made of single constituent components. Consider that the three-dimensional (3D) nanocarbon-based foams usually consist of 2D cell walls; synergetic enhancement of the mechanical performance is thus expected in hybrid foams constructed by both CNT and graphene. Recently, attempts to combine CNT and graphene have been made to fabricate 3D hybrid cellular solids; however, most of them are focused on the electrochemical properties such as capacity, only a few reports addressing mechanical response of them exist.[20-25] For instance, Gao and co-workers fabricated a ultra-flyweight carbon aerogel through building a framework with giant graphene flakes and CNT building blocks. However, the random organized structures in their materials, caused isotropic properties, behaved a negative unloading stress when subjected to compression, indicating incomplete elasticity.[24] Thus, to harness the extraordinary mechanical properties of building blocks effectively, fabricating CNTs and graphene hybrid foams with ordered structural manner and synergistic combination of mechanical compressibility, elasticity and stability still remains as a challenge.

Herein, we fabricated CNT/graphene hybrid foams with highly ordered hierarchical architectures by applying unidirectional freeze-casting method. The as-prepared hybrid foam shows an ordered honeycomb-like structure, in which graphene and CNT components are well interwoven and stacked within the cell wall. Symmetrical mechanical tests on these hybrid foams revealed their superb properties of combining high specific strength, elasticity, compressibility, and dynamic mechanical stability when compared with neat CNT or graphene foams, which also cannot achieved by graphene/CNT hybrid foam with poorly organized structures.[24] Such remarkable mechanical performance is attributed to the synergistic-effects-induced highly organized, multi-scaled hierarchical architectures at different levels, which providing enhanced cell walls strength and stability. At last, combining with the electrical conductivity, the hybrid foam show the capability as a flexible pressure sensors. We further demonstrated their potential application in artificial skin fields by integrated graphene foams into pixel arrays.

Experimental Section

Materials

Graphite powder with a size of 20 μm was purchased from Qingdao Yingshida Graphite Co. Ltd. MWCNT (6-8 nm in diameter, up to 50 μm in length, and purity >93 wt.%, FloTubeTM7000) was bought from CNano Technology Ltd. Analytical grade $NaNO_3$, $KMnO_4$, 98% H_2SO_4, 69% HNO_3 and 30% H_2O_2 aqueous solution were purchased from Beijing Chemical Works and were used directly without further purication.

Fabrication of CNT, graphene and hybrid foams

GO was prepared by a modified Hummer's method.[26] The prepared GO suspension of various concentrations was poured into a Teflon cubic container with a stainless steel bottom. Unidirectional growth of ice from the bottom to the upper face occurred when the container's stainless steel bottom was immersed in liquid nitrogen. The frozen GO suspension was then transferred into a freeze-drying vessel (-50 ℃ and 20 Pa) and freeze-dried for 24 h to obtain a macroporous GO foam. To obtain the graphene foam, the GO foam was placed in a tube furnace and annealed at 800 ℃ for 3 h under an argon atmosphere.

o-CNT (chemically oxide CNT) was synthesized according to the chemical method reported in reference[27] but with short oxide time that is CNT refluxed in the mixture of concentrated H_2SO_4 and HNO_3(3:1 by volume) for only 15 min, and then collected by repeated centrifuging and washing with deionized water. At last, we obtained the *o*-CNT aqueous. In this step, the oxygen content of *o*-CNT is important to the final foams properties that lower content would render the foam with better mechanical properties. Following the similar procedures for making graphene foam, we obtained the CNT foams.

When mixing the two solutions together with different weight ratio and obeying the above-mentioned methods we obtained the hybrid foams.

Characterization

The microstructure and morphology of the as-prepared foams were characterized by SEM (HITACHI S4800). Spectral analysis of GO and *o*-CNT was characterized by FTIR spectroscopy (Spectrum One, PE, US). A dynamic mechanical analyzer (TA, DMA Q800) was used to evaluate the mechanical performance of the foams. The dimensions of the tested samples were 1 cm×1 cm × 1 cm. We combine home-made mechanical tester and SEM (HITACHI S3400) to in-situ observe the compressive behavior of the foams. Electrical properties were tested using Keithley 4200 SCS in the four-probe mode. The top and bottom surfaces of the foam were coated with a uniform layer of silver paste and the side faces were coated with two strip of silver paste. Four silver wires were connected to these sliver paste respectively. For the electromechanical tests, the top and bottom surfaces of the ReG foam were coated with a uniform layer of silver paste and connected by silver wires. During the compression process, the

electrical resistance (Keithley 4200 SCS under a bias of 10 mA) was recorded simultaneously.

Results and discussion

Built graphene and CNT based foams via freeze casting

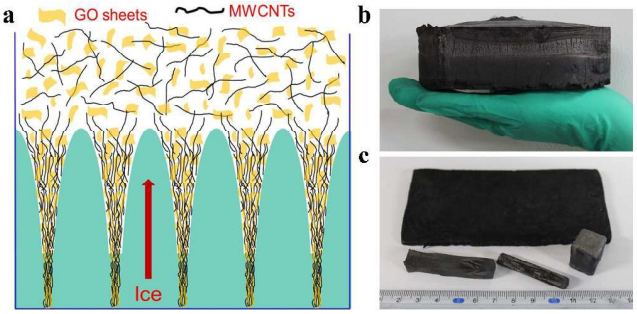

Figure 1. Illustration of fabrication technique of foams. (a) When a well-dispersed GO/*o*-CNT dispersion is frozen, nanobuilding blocks are concentrated at the boundary of ice crystals and then aligned along the growth direction of ice due to the squeezing effect. Consequently, stable macrostructures are formed and survived after freeze drying followed by thermal annealing. Benefiting from the technique, we can prepare samples with different shape and size. Photos of the corresponding samples are presented in (b,c).

Freeze casting methods, have received significant interests over the past decade due to the compelling advantages of inexpensiveness, versatility and one-step process, and are being successfully adopted to synthesize a variety of porous ceramic, metallic, polymeric and composite materials, including recent reported CNT or graphene-based foams.[28-30] During the freeze casting process, particles entrapped in aqueous solution were ejected from the moving solidifying front of the ice crystal and then piled up between the growing columnar or lamellar ice crystals. **Figure 1a** presents the schematic drawing of self-assembly process of nanostructured carbon materials based cellular solids, in which individual nanomaterials were ejected from the front of the ice crystal and assembled between the growing columnar or laminar ice. After the subsequent sublimation of ice crystals by the freeze-drying technique, stable free-standing three dimensional foams were obtained. In order to get homogenously dispersed aqueous CNT and/or graphene solutions, the precursors for freeze casting, CNT and graphite were oxidized firstly according to previous publications.[26, 27] Our prepared oxidized CNT (*o*-CNT) and graphene oxide (GO) can be dispersed in the water quite well due to the attachment of amount of oxygen containing groups such as hydrogen, epoxy and carboxyl (FTIR characterization shown in **Figure S1**). Here, we fabricated various nanostructured carbon materials based macroscopic foams including *o*-CNT, GO and *o*-CNT/GO hybrid foams by freeze-casting of corresponding aqueous solutions (Figure 1a, Experimental Section), followed by thermal annealing to remove the oxygen contained groups and endow the materials with good electrical conductivity and good elasticity.[30] As showed in Figure 1b and 1c, the macroscopic-assembled foams with controlled size (up to 800 cm^3) and shape such as cubes, cylinders and plates were readily accessible.

Figure 2a to **2i** presents the typical microscope (SEM) images of all three types of foams, exhibiting anisotropic structural features, longitudinally channel like morphology and transverse honeycomb-like morphology with the cell dimension in the order of tens of micrometers. The cell walls are slightly corrugated and have a thickness of tens of nanometers. Such a high ratio of channel width to wall thickness, approximately 10^3, produces the foams with ultra-low density and extra-high porosity. Consistent with our previous report,[30] graphene foam show morphology of short channels with joint walls along the growth direction in Figure 2a. In addition, polygon pores with defects (as shown by arrows in Figure 2g) in the walls and edges are observed in Figure 2d and 2g. Unlike graphene foam, CNT foams possessed long straight channels without joint walls along the growth direction (Figure 2b) and polygon pores which composed with less-defected cell walls and edges in the cross-section images (Figure 2h), which similar to those of previous report.[1, 8, 31] Of particular interest is that by mixing these two kinds of building blocks together, an optimized structure is obtained in the hybrid foams: ordered honeycomb-like structures with joint walls in the growth direction and less-defected cell walls and edges in cross-section view (Figure 2c, 2f and 2i).

Earlier works have revealed that the microstructural features of the cellular solids as-prepared from freeze casting method are governed by the complex and dynamic liquid-particle and particle-particle interactions.[32] The particles with different surface chemistry and geometries would play a significant effect on the microstructures of the resulting foams.[10, 33] Herein, the plate-like geometry of GO sheets and stronger interaction between the sheets with water solvents which attributed to the large amounts of oxygen-containing groups on the sheets would result in steric hindrance effect during the assembly process, and then part of GO sheets were entrapped in the ice crystal front, and eventually lead to the formation of joint walls in the channels. Meanwhile, the steric effects on restack of the sheets also led to the formed defects in the walls and junctions between them. Alternatively, spaghetti-like *o*-CNT with lower oxidization degree (see experiment part) has negligible hindrance effect on the growth of the ice crystal, and hence, the morphology of CNT-based foams is prone to form the ordered structure with good regularity. After combining of *o*-CNT and GO components together in aqueous solutions, *o*-CNT tends to absorb on the graphene oxide sheets through π-stacking interaction.[34] Thus, the hybrid foam shows the honeycomb-like framework similar to that of neat graphene foam.

Mechanical properties

The ability to maintain structural integrity upon large deformation for graphene or CNT based foams is important for future development of carbon-based flexible materials, ultra-light engineering cellular materials for mechanical damping an new types of flexible electronic devices. According to our previous work,[30] the foams always show better mechanical

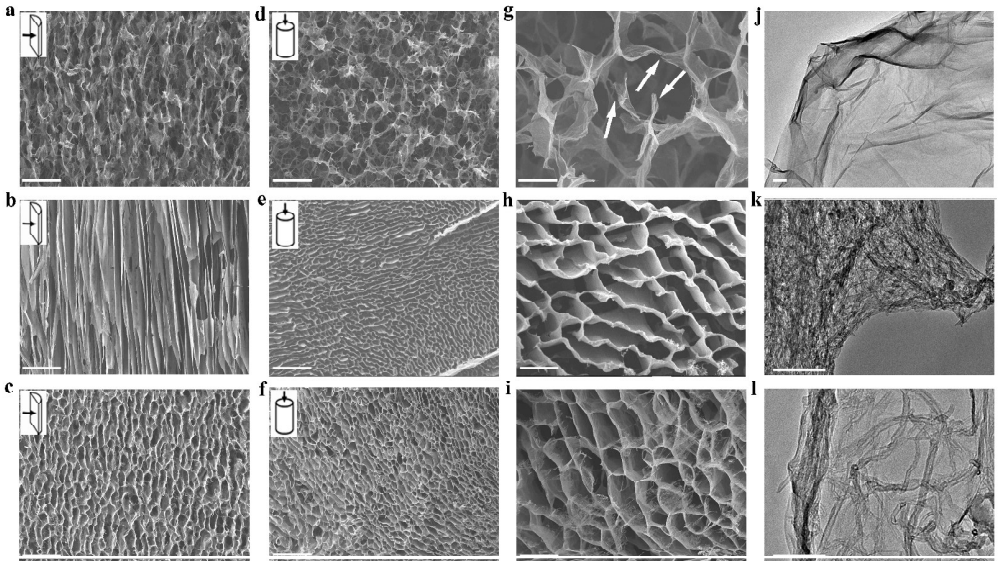

Figure 2. SEM images showing longitudinal (a) and cross-section views of the as-prepared graphene foam (d,g), white arrows show defects on the walls and junction in the graphene foam ; Microstructures of CNT foam and hybrid foam along the longitudinal direction(b,c) and in cross-sectional area (e,f). In the hybrid foam, the defect is less than that in graphene foam. Moreover, we can find the pull-out CNT bundles. TEM images of the walls in the three kinds of foams. the cell walls in graphene foam were consisted of wrinkled and overlapped graphene sheets (j); In CNT foams the walls are spaghetti-like networks with entangled random distributed nanotubes (k) and in hybrid foam the spaghetti-like CNT networks cover on the graphene sheets form sandwich structures (l), Scale bar in a-f: 100 μm, in g-i: 20 μm, in j-k : 200 nm, in l: 100 nm.

compressibility and mechanical stability when the load are applied perpendicular to the growth (in-plain) direction and hence the in-plain-direction mechanical performance is particularly explored in this work. **Figure 3a** shows the compressive stress-strain curves for all three samples. Curves obtained during the loading process show the three characteristic deformation regimes typically observed in open-cell foams. A linear regime for strain $\leqslant$ ~10% is generally reflect the elastic bending of cell walls. Elastic buckling of cell walls is recorded by a plateau regime with gradually increasing slop after plateau strain (~10%) and a densification regime for strain > ~50% with steeply rising stress.[3] While conventional foams displayed permanent deformation during plateau regime, graphene foams could hold their elasticity before densification and irreversible compressive deformation only appears at large strain (Supporting Information **Figure S3**). The strength of the graphene foam as quantified by plateau stress at 20% strain to density (1.8-5.4 mg/cm^3) ratio, is ~0.11 kPa/mg•cm^{-3} which is similar to that of graphene based foam in literature.[35, 36] Compared with graphene foams, CNT foams exhibit intriguing structural compressibility, with achieving nearly full recovery from large strains ($\geqslant$ 90%) under uniaxial loading which is also observed in previous CNT aerogels fabricated with the assistant of polymer binder.[8] However, the specific strength of CNT foams is only ~0.01 kPa/mg•cm^{-3} which is much lower than that of as-formed graphene foams. Surprisingly, due to their synergistic effect, the CNT/graphene hybrid foam shows the highest specific strength (~0.35 kPa/mg•cm^{-3}) without any trade-off in the compressibility as shown in Figure 3a and **Figure S4**. It was worth noting that the weight ratio of the graphene to CNT also have crucially effect on their mechanical properties. By carefully control the ratio between the two parts we found that the hybrid foam in 1:1 weight ratio possess the best mechanical performance as illustrated in **Figure S5**. Therefore in the following parts, we only focus on the properties of hybrid foam with ratio 1:1.

Cyclic tests of hybrid foams with large amplitude (60% strain) were conducted by compression at 0.017 Hz. Figure 3b shows identical stress-strain behavior of foams after 2000 cycles, indicating little loss of long-term strength and excellent mechanical stability. Our previous work has shown that graphene foams would experience 6% stress degradation at 60% after only 100 cycles.[30] After the addition of CNT, synergistic effects make the hybrid foams resistant to dynamic loading and dynamic load bearing capacity is successfully improved. Only ~5% degradation was measured at 60% strain after 1000 cycles in the hybrid foams, in stark contrast to that of CNT/graphene hybrid aerogels with poorly organized structure (12% stress degradation at only 50% strain after 1000 cycles) and the neat hierarchical graphene foam (19% stress degradation at 50% strain after 1000 cycles),[10, 24] which should attribute this super mechanical stability to the hybrid solid constituents and the highly improved structural regularity in our materials.

This excellent loading bear capacity of our hybrid foams could be also displayed in the unloading curves in cyclic tests, in which three characteristic deformation regimes could be also observed. By contrast, the three regimes disappeared in unloading stress-strain curves of most of nanostructured carbon

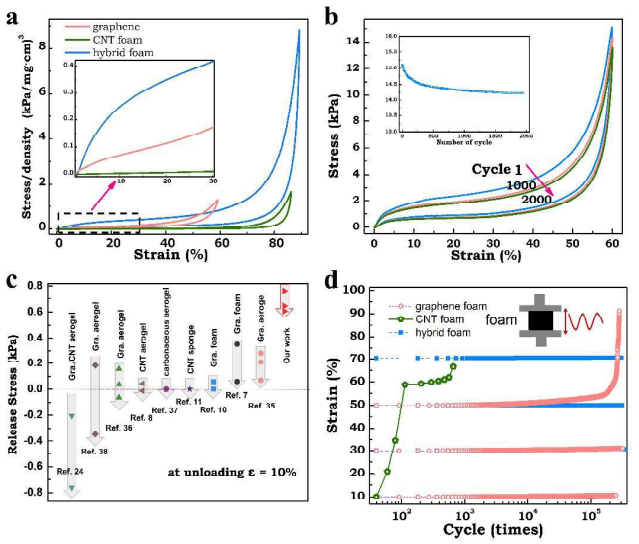

Figure 3. Characterization of mechanical properties of as-formed foams. (a) Stress-strain curves for graphene foam, CNT foam and hybrid foam. The density of samples is ~6-~8 mg/cm^3, and the influence of density on the stress-strain curves were investigated in Supporting Information Figure S4. (b) Stress-strain curves of hybrid foam at 1th, 1000th and 2000th cycles during repeated compression to 60%. Insert: stress recorded at 60% strain for 2000 cycles compression showing excellent cycle performance of hybrid foam. The compression and release speed is 120%/min. (c). Comparison of the stress value at 10% strain of hybrid foams and other materials in unloading stress-strain curves during cyclic test. Note that the performance of most of materials would be different with different densities and loading directions (anisotropy) and we chose the highest value (best performance) as their loading bear value. The arrows showed the decreased stress with the increasing cycle numbers, we can find the good mechanical stability in the unloading process of our samples. (d). The fatigue resistance of the three kinds of foams at different strain levels. Insert: schematic of compressive cyclic testing. Strikingly, hybrid foam possesses quite good fatigue resistance even at set strain of 70%.

based foams or aerogels and the stress would drop to zero or even a negative value during unloading, indicating incomplete elasticity. Figure 3c shows a comparison of the loading bearing capacity of our hybrid foam and other recently reported 3D porous materials, including graphene foams,[10, 36] graphene aerogels,[7, 35] carbonaceous aerogels,[37] CNT aerogels,[8] CNT sponges,[11] graphene sheets-nanoribbon aerogels[38] and CNT/graphene hybrid aerogels[24] under cyclic loading. It was found that the hybrid foams show better unloading performance when compared with other cellular solids in Figure 3d. For instance, for the unloading stress at 10% strain, most of materials experiences severely degradation with increasing cycles, our hybrid foams hold most of the load after 2000 cycles and showed the super-elasticity and excellent loading bear capacity as shown in Figure 3c.

Dynamically compressive testing with strain amplitude (5%) at 10 Hz were further employed to assess the fatigue performance of these foams at various applied strain levels for at least 2.0 × 10^5 cycles (Figure 3d). Although their excellent compressibility at static compression, due to the low strength and poor load bearing capacity, CNT foams would collapse at low compression strain (10%) after less than one hundred cycles as evidenced by the large fatigue strain (shrinkage from the original length) in Figure 3d. Comparatively, graphene foams showed much better structural robustness and exhibited negligible fatigue strain at low strain level. Note, however, at the set strain of 50%, the shrinkage of graphene foams began to increase rapidly after 10 thousand cycles as shown in Figure 3d, which could be considered as fatigue failure or degradation. Strikingly, it is found that the fatigue performance of hybrid foams are remarkably stable and only 0.61% fatigue shrinkage could be measured after enduring 300 thousand of cycles at large strain (70%), highlighting their structural robustness and fatigue resistance. Additionally, it is worth noting that our hybrid foams also exhibit dynamic thermo-mechanical stability, as evidenced by constant storage modulus over a wide temperature range (-150-350 ℃) in **Figure S6**, further promising their practical application as lightweight, robust and elastic cellular materials with stable performance in extreme conditions.

Synergistic mechanism

As nanostructured carbon-based macroscopic porous architectures are generally brittle with low mechanical resilience and permanent deformation could usually be observed after severe compression, the exceptional static and dynamic mechanical performance observed in our CNT/graphene hybrid foams was a surprise to us. Previous studies suggest that when foam made of graphene or CNT based walls is severely compressed, locally damaged microstructure by collapsing and overwhelmed elastic energy by the inter-wall adhesion such as van der Waals interaction would prevent elastic recovery, causing loss of collective elasticity and strength.[10] Indeed, the super-elasticity and mechanical stability could not be observed in neat graphene foams (Figure, S7, S8c and d) with poor ordered structure or graphene/CNT hybrid aerogels with random stacking.[24] We thus believe that, in our hybrid materials, the highly organized, hierarchical architectures and the synergistic-effects at different levels are contributed to such remarkable mechanical performance. By monitoring the deformation process of hybrid foam, the contributions of every structural level to the improved mechanical stability are discussed from the following three aspects:

Firstly, structural regularity in the hybrid foams allows the homogeneous structural reorganization under increasing compressive strain as shown in situ compression SEM images in **Figure 4a**. When uniaxial stress is initially applied to the foams so that each cell edge would transfer the force, the structure deformation was activated and the walls in one cell began bending and buckling. Due to their ordered organization, the structure in hybrid foams exhibits uniform deformation, whereas the non-uniform distribution of cell size in randomly structured foams leads to inhomogeneous strain and locally severe deformation. As shown in Figure S7 and S8, both locally structural damage and unrecovered deformation are observed in graphene foam and, by contrast, the hybrid foams still hold their honeycomb-like structure after 90% compression. In addition, this honeycomb-like manner in which the nanostructured carbon materials based walls are organized

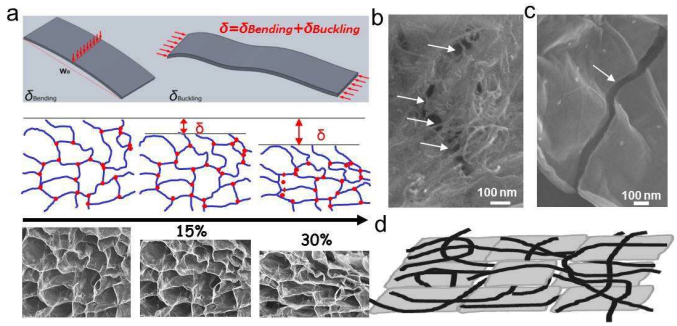

Figure 4. (a). Schematic description of the unit cell model of the foams and the evolution in cell structure with strain. The foam exhibits uniform deformation. SEM images illustrate the morphology of the cracks on the cell walls. (b). In the hybrid foam the CNT bundles connect the cleft parts together, (c) while in the graphene foam, smooth crack was observed, which imply their lower stability. (d) Schematic drawing of the cell walls which are comprised of stacked graphene sheets and the intercalated spaghetti-like nanotubes.

was also considered to be able to maximize the elastic modulus and strength.[10]

Secondly, the mechanical stability of cell edges was crucially important to guarantee the structural compressibility and elasticity under large deformation. According to the structural characterization as shown in Figure 2g and Figure S7b, the presence of apparent defects in cell edges would greatly weaken the strength and stability of the graphene foam. After incorporation of nanotube inside graphene sheets, the defects in edges between neighbouring cell walls in hybrid foam were significantly eliminated (figure 2i).

Thirdly, in the hybrid foams, the cell walls are comprised of stacked graphene sheets and spaghetti-like nanotubes as shown schematic diagrams in Figure 4d. Expectedly, nanotubes behaved like long and entangled threads to weave graphene sheets into continuous structures, and then greatly enhanced its microstructure stability under static and dynamic compression. For instance, one of deformation modes observed in the cell wall depended on crack prorogation as shown in Figure 4b and 4c. Like the fibrils induced crack–shielding mechanism in biomaterials, the nanotubes, interweaving in the crack zone and acts as fiber bridges, is effective against propagation of cracks and advance in damage zone.[39] Meanwhile, according to the literature,[18, 40] we also suggest that mechanical properties such as strength and modulus of the solid constituents (cell walls) in the hybrid foams would be enhanced, allowing the van der Waals adhesion to be overcome by the elastic energy. Therefore, combination of compressibility, super-elasticity and stability performance in our hybrid foams should be contributed to the synergistic effects from graphene and carbon nanotubes, by which ordered, multi-scaled hierarchical architectures could be achieved and both the bending stiffness and damage resistance of the solid constituents in this architecture under compression are improved effectively.

Pressure sensor and application in artificial skin

The graphene and carbon nanotubes construct hybrid foams not only with excellent mechanical properties but also with high electrical conductivity. Four-probe electrical tests indicated that the electrical conductivity of the hybrid foam could reach up to ~0.2 S/cm, which is close to that of graphene foam in our previous work,[30] holding great potential for applications as pressure sensors in smart material fields. In order to demonstrate its sensor capability, the variation of electronic resistance to the applied pressure at different situation was investigated as shown in **Figure 5a**. The resistance variation ratios (defined as $\triangle R/R_0 = (R_p-R_0)/R_0$ where R_0 and R_p denote the electrical resistance without and with applied pressure, respectively) increased monotonously with the loading at lower pressure range up to 2.5 kPa, after that the increased trend of $\triangle R/R_0$ turned negligible with applied pressure. The decreased resistance of hybrid foam during the compression process was mainly due to the varied conducting paths and contact resistance between the nearby cell walls. Specifically, the pressure sensitivity S (defined as $S= \delta (\triangle R/R_0)/ \delta_P$, here P is the applied pressure) is 0.19 kPa^{-1} , 0.02 kPa^{-1} in the 0-2.5 kPa and 2.5-13 kPa range under loading process respectively. After removing the applied pressure, the electrical resistance completely recovers to its original value, indicating its ability to detect the pressure cyclically. Comparatively, the S value in lower pressure level is almost one order of magnitude higher than that of CNT/PDMS sponge (S=0.023 kPa^{-1}) as well as CB/PDMS sponge (S= 0.046 kPa^{-1}) in literature.[41, 42] Also, it is comparable to that of graphene coated PU foam based pressure sensor (S = 0.26 kPa^{-1})[43] or complicated micro- or nano-structure pattern based sensors from 0.55 kPa^{-1} up to 8.4 kPa^{-1}.[44, 45](more information were illustrated in Table S1 in the

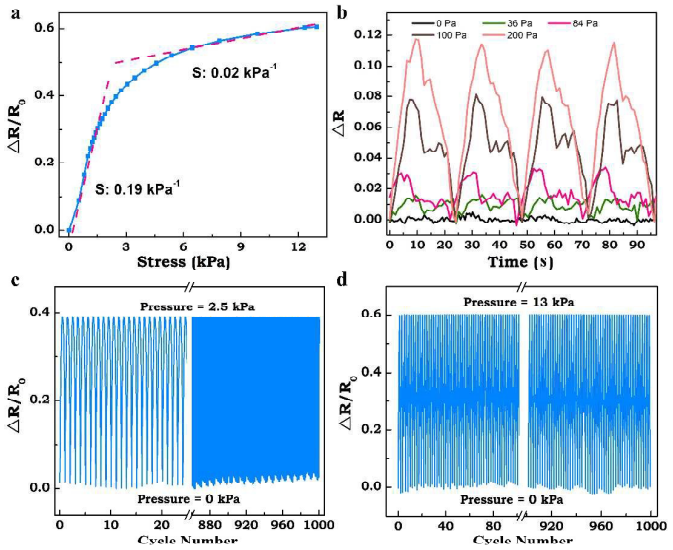

Figure 5. Characterization of the resistive pressure response of hybrid foam: (a) electric variation ratio change with applied pressure. The ratio increased exponential with the increased pressure; the sensitivity in the range of 0-2.5 kPa is 0.19 kPa^{-1}, while in the range of 2.5-13 kPa is 0.02 kPa^{-1}. (b) Detection limit test on the hybrid foam. The minimum value of the detectable pressure is 36 Pa. Reliability test of hybrid foam under repeated loading and unloading pressure of 2.5 kPa (c) and of 13 kPa (d).

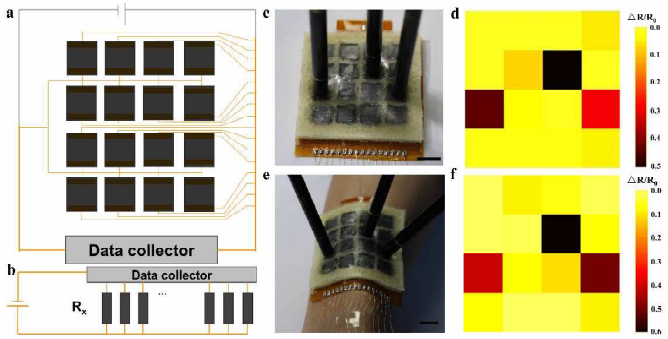

Figure 6. Schematic model of the artificial skin. The hybrid foams (black squares) were attached on the electrodes (yellow rectangles). And the signals were collected by the data collector (a). The equivalent circuit of the sensor. R_x represents the dynamic resistance of the hybrid foam during the loading process (b). Photographs of the artificial skin, and three positions were compressed to test the pressure-sensing capability (c). The mapping profile of the pixel signals generated by the compression (d). Photographs of the artificial skin attached on arm and three positions were compressed (e). The mapping profile of the pixel signals generated by the compression (f). Scale bar : 10 mm.

supporting information).However, in the former case, fractures in PU foams are required to improve the pressure sensitivity, accompanying apparent decrease in mechanical stability. For the latter, both the size and shape of the micro-structured rubber layers based core part in the sensors have to be carefully controlled to fulfil their function.

To further investigate the features of the sensor, the resistive responses of the foam to cyclic loading and unloading at set pressures were recorded and plotted in Figure 5b. It clearly shows that this sensor can detect pressure as low as 36 Pa, which is comparable to the detectable pressure values achieved by other types of pressure sensors (see Table S1) in literature: 3 Pa,[44] 9 Pa,[43] 27 Pa,[46] 2.5 kPa,[47] 50 kPa.[48] Regarding the potential application as pressure sensors, the structural stability of the foam is one of the major performances considered. To this end, cycle tests with two pressure ranges that are 2.5 kPa and 13 kPa over one thousand times (in Figure 5c,d) were applied to the sensors. The consistent resistance variation can be maintained during the process, implying their long working life and reliability.

In addition, we demonstrated the as-prepared graphene/CNT hybrid foams can be integrated into a flexible device utilized in artificial skin fields. As illustrated in **Figure 6**, the hybrid foams with size of 8×8×4 mm^3 were attached on the Polyimide (PI) film which equipped previously with electrodes to form a 4×4 pixel arrays. The schematic model and photograph of the sensor were shown in Figure 6a, 6c and 6e. The boundary among the individual graphene/CNT foam units were separated by PU foam, and sealed by PDMS film. The pressure-sensing mechanism of our device is related to the resistive variation of the foam between the counter electrodes. The equivalent circuit of the obtained electronic sensor is shown in Figure 6b; in which R_x represent the dynamic resistance of the foam between the electrodes. When the pressure was applied to the individual arrays in the device in Figure 6c, the one that pressure applied exhibited deformation which leading to the decrease of the local resistance, while the neighbouring arrays which have not encountered the compression still would keep their initial states. Mapping out the resistive variation of individual arrays would clearly show the pressure distribution in the devices as shown in Figure 6d, implying its high space resolution and pressure sensitivity. Comparatively, the device configuration in this work exhibit high pressure and spatial sensitivity, which cannot be achieved in the graphene/PU foam based pressure device because of their inevitable mutual interference among the units as reported in Yu's work.[43] Figure 6e shows the device can also detect the pressure under bending situation, where both the spatial resolution and pressure intensity are similar to that of flat situation. In fact, the space resolution is limited by the size of the foam units. In the future, the device with much higher resolution such as down to micro- or nano-scale would be achieved via making tiny foams.

Conclusions

In this study, we have successfully fabricated hierarchically structured graphene/CNT hybrid foams through freeze casting methods followed by thermal reduction. The ideal combination of the two types of nanostructured carbon materials bring multi-scale synergistic effects in the hierarchical ordered structure which offer the as-prepared foam outstanding mechanical performance, such as super elasticity, compressibility, stability and highest mechanical strength. Along with their good electrical conductivity, we revealed their capability in detecting pressure with high sensitivity and long life time. Equipped with flexible electric circuit, we successfully demonstrated its potential as artificial skin.

Acknowledgements

This project was jointly supported by the National Key Basic Research Program of China (Grant Nos 2012CB937503 and 2013CB934203) and the National Natural Science Foundation of China (Grant Nos. 51173030, 11225210, 21474023 and

11222217). And thank you for the kindly help from Prof. Deyi Kong in Institute of Intelligent Machines, Chinese Academy of Sciences for the design of the circuit.

Notes and references

[a] National Center for Nanoscience and Technology, China, Beijing 100190, China. E-mail: liulq@nanoctr.cn; zhong.zhang@nanoctr.cn

[b] University of Chinese Academy of Sciences, Beijing 100049, China.

[c] School of Materials Science and Engineering, University of Science and Technology of Beijing, Beijing 100083, China..

† Electronic Supplementary Information (ESI) available. See DOI: 10.1039/b000000x/

1. A. Abarrategi, M. C. Gutiérrez, C. Moreno-Vicente, M. J. Hortigüela, V. Ramos, J. L. López-Lacomba, M. L. Ferrer and F. del Monte, *Biomaterials*, 2008, **29**, 94-102.
2. M. Avalle, G. Belingardi and R. Montanini, *Int. J. Impact. Eng.*, 2001, **25**, 455-472.
3. L. J. Gibson and M. F. Ashby, *Cellular solids: structure and properties*, Cambridge university press, 1999.
4. M. I. Idris, T. Vodenitcharova and M. Hoffman, *Mater. Sci. Eng., A*, 2009, **517**, 37-45.
5. S. Nardecchia, D. Carriazo, M. L. Ferrer, M. C. Gutiérrez and F. del Monte, *Chemical Society Reviews*, 2013, **42**, 794-830.
6. H. Huang, P. Chen, X. Zhang, Y. Lu and W. Zhan, *Small*, 2013, **9**, 1397-1404.
7. Y. R. Li, J. Chen, L. Huang, C. Li, J. D. Hong and G. Q. Shi, *Adv. Mater.*, 2014, **26**, 4789.
8. J. Zou, J. Liu, A. S. Karakoti, A. Kumar, D. Joung, Q. Li, S. I. Khondaker, S. Seal and L. Zhai, *ACS Nano*, 2010, **4**, 7293-7302.
9. Y. Xu, K. Sheng, C. Li and G. Shi, *ACS Nano*, 2010, **4**, 4324-4330.
10. L. Qiu, J. Z. Liu, S. L. Chang, Y. Wu and D. Li, *Nat. Commun.*, 2012, **3**, 1241.
11. X. Gui, A. Cao, J. Wei, H. Li, Y. Jia, Z. Li, L. Fan, K. Wang, H. Zhu and D. Wu, *ACS Nano*, 2010, **4**, 2320-2326.
12. Z. Chen, W. Ren, L. Gao, B. Liu, S. Pei and H. M. Cheng, *Nat. Mater.*, 2011, **10**, 424-428.
13. R. R. Kohlmeyer, M. Lor, J. Deng, H. Liu and J. Chen, *Carbon*, 2011, **49**, 2352-2361.
14. M. B. Bryning, D. E. Milkie, M. F. Islam, L. A. Hough, J. M. Kikkawa and A. G. Yodh, *Adv. Mater.*, 2007, **19**, 661-664.
15. M. A. Worsley, P. J. Pauzauskie, T. Y. Olson, J. Biener, J. H. Satcher and T. F. Baumann, *J. Am. Chem. Soc.*, 2010, **132**, 14067-14069.
16. W. Chen and L. Yan, *Nanoscale*, 2011, **3**, 3132-3137.
17. M. K. Shin, B. Lee, S. H. Kim, J. A. Lee, G. M. Spinks, S. Gambhir, G. G. Wallace, M. E. Kozlov, R. H. Baughman and S. J. Kim, *Nat. Commun.*, 2012, **3**, 650.
18. Z. D. Huang, B. A. Zhang, S. W. Oh, Q. B. Zheng, X. Y. Lin, N. Yousefi and J. K. Kim, *J. Mater. Chem.*, 2012, **22**, 3591-3599.
19. Y. W. Cheng, S. T. Lu, H. B. Zhang, C. V. Varanasi and J. Liu, *Nano Lett.*, 2012, **12**, 4206-4211.
20. X. C. Dong, J. Chen, Y. W. Ma, J. Wang, M. B. Chan-Park, X. M. Liu, L. H. Wang, W. Huang and P. Chen, *Chem. Commun.*, 2012, **48**, 10660-10662.
21. X. C. Dong, Y. W. Ma, G. Y. Zhu, Y. X. Huang, J. Wang, M. B. Chan-Park, L. H. Wang, W. Huang and P. Chen, *J. Mater. Chem.*, 2012, **22**, 17044-17048.
22. W. Wang, S. R. Guo, M. Penchev, I. Ruiz, K. N. Bozhilov, D. Yan, M. Ozkan and C. S. Ozkan, *Nano Energy*, 2013, **2**, 294-303.
23. A. P. Cohn, L. Oakes, R. Carter, S. Chatterjee, A. S. Westover, K. Share and C. L. Pint, *Nanoscale*, 2014, **6**, 4669-4675.
24. H. Sun, Z. Xu and C. Gao, *Adv. Mater.*, 2013, **25**, 2554-2560.
25. Z. Fan, J. Yan, L. Zhi, Q. Zhang, T. Wei, J. Feng, M. Zhang, W. Qian and F. Wei, *Adv. Mater.*, 2010, **22**, 3723-3728.
26. L.-Q. L. Yun Gao, Sheng-Zhen Zu, Ke Peng, Ding Zhou, Bao-Hang Han, and Zhong Zhang, *ACS Nano*, 2011, **5**, 2134–2141.
27. J. Zhang, H. Zou, Q. Qing, Y. Yang, Q. Li, Z. Liu, X. Guo and Z. Du, *The Journal of Physical Chemistry B*, 2003, **107**, 3712-3718.
28. S. Deville, E. Saiz and A. P. Tomsia, *Acta Mater.*, 2007, **55**, 1965-1974.
29. H. Zhang and A. I. Cooper, *Adv. Mater.*, 2007, **19**, 1529-1533.
30. J. Kuang, L. Liu, Y. Gao, D. Zhou, Z. Chen, B. Han and Z. Zhang, *Nanoscale*, 2013, **5**, 12171-12177.
31. M. a. J. H. e. Marı´a C. Gutie´rrez, J. Manuel Amarilla, Ricardo Jime´nez, and a. F. d. M. Marı´a L. Ferrer, *The Journal of Physical Chemistry C*, 2007, **111**, 5557.
32. S. Deville, *Adv. Eng. Mater.*, 2008, **10**, 155-169.
33. W. Li, K. Lu and J. Walz, *Int. Mater. Rev.*, 2012, **57**, 37-60.
34. C. Zhang, L. Ren, X. Wang and T. Liu, *J. Phys. Chem. C*, 2010, **114**, 11435-11440.
35. H. Hu, Z. Zhao, W. Wan, Y. Gogotsi and J. Qiu, *Adv. Mater.*, 2013, **25**, 2219-2223.
36. S. Barg, F. M. Perez, N. Ni, P. do Vale Pereira, R. C. Maher, E. Garcia-Tunon, S. Eslava, S. Agnoli, C. Mattevi and E. Saiz, *Nat Commun*, 2014, **5**, 4328.
37. X.-L. Wu, T. Wen, H.-L. Guo, S. Yang, X. Wang and A.-W. Xu, *ACS Nano*, 2013, **7**, 3589-3597.
38. C. Wang, X. He, Y. Shang, Q. Peng, Y. Qin, E. Shi, Y. Yang, S. Wu, W. Xu, S. Du, A. Cao and Y. Li, *J. Mater. Chem.A*, 2014, **2**, 14994-15000.
39. R. O. Ritchie, *Nat. Mater.*, 2011, **10**, 817-822.
40. Q. Liu, L. Liu, J. Kuang, Z. Dai, J. Han and Z. Zhang, *Nanoscale*, 2014, **6**, 6932-6938.
41. J.-W. Han, B. Kim, J. Li and M. Meyyappan, *Appl. Phys. Lett.*, 2013, **102**, 051903.
42. M. G. King, A. J. Baragwanath, M. C. Rosamond, D. Wood and A. J. Gallant, *Procedia Chemistry*, 2009, **1**, 568-571.
43. H. B. Yao, J. Ge, C. F. Wang, X. Wang, W. Hu, Z. J. Zheng, Y. Ni and S. H. Yu, *Adv. Mater.*, 2013, **25**, 6692-6698.
44. S. C. B. Mannsfeld, B. C. K. Tee, R. M. Stoltenberg, C. V. H. H. Chen, S. Barman, B. V. O. Muir, A. N. Sokolov, C. Reese and Z. Bao, *Nat. Mater.*, 2010, **9**, 859-864.
45. G. Schwartz, B. C. K. Tee, J. Mei, A. L. Appleton, D. H. Kim, H. Wang and Z. Bao, *Nat. Commun.*, 2013, **4**, 1859.
46. C.-L. Choong, M.-B. Shim, B.-S. Lee, S. Jeon, D.-S. Ko, T.-H. Kang, J. Bae, S. H. Lee, K.-E. Byun, J. Im, Y. J. Jeong, C. E. Park, J.-J. Park and U. I. Chung, *Adv. Mater.*, 2014, **26**, 3451-3458.
47. I. Manunza, A. Sulis and A. Bonfiglio, *Appl. Phys. Lett.*, 2006, **89**, 143502.
48. D. J. Lipomi, M. Vosgueritchian, B. C. K. Tee, S. L. Hellstrom, J. A. Lee, C. H. Fox and Z. Bao, *Nat. Nanotechnol.*, 2011, **6**, 788-792.

